Vol 18 No 7, July 2009
1674-1056/2009/18(07)/3024-07

Chinese Physics B

© 2009 Chin. Phys. Soc.
and IOP Publishing Ltd

Synthesis and electrical characterization of tungsten oxide nanowires*

Huang Rui(黄 睿), Zhu Jing(朱 静)†, and Yu Rong(于 荣)

Beijing National Center for Electron Microscopy, The State Key Laboratory of New Ceramics and Fine Processing, Laboratory of Advanced Materials, Department of Materials Science and Engineering, Tsinghua University, Beijing 100084, *China*

(Received 24 November 2008; revised manuscript received 16 December 2008)

Tungsten oxide nanowires of diameters ranging from 7 to 200 nm are prepared on a tungsten rod substrate by using the chemical vapour deposition (CVD) method with vapour–solid (VS) mechanism. Tin powders are used to control oxygen concentration in the furnace, thereby assisting the growth of the tungsten oxide nanowires. The grown tungsten oxide nanowires are determined to be of crystalline $W_{18}O_{49}$. *I–V* curves are measured by an *in situ* transmission electron microscope (TEM) to investigate the electrical properties of the nanowires. All of the *I–V* curves observed are symmetric, which reveals that the tungsten oxide nanowires are semiconducting. Quantitative analyses of the experimental *I–V* curves by using a metal–semiconductor–metal (MSM) model give some intrinsic parameters of the tungsten oxide nanowires, such as the carrier concentration, the carrier mobility and the conductivity.

Keywords: tungsten oxide nanowires, chemical vapour deposition (CVD), electrical characterization, metal–semiconductor–metal (MSM) structure

PACC: 7360P, 6140M, 7340S

1. Introduction

Compared with other transition metal oxides, tungsten oxides have attracted great attention and have been investigated extensively due to their outstanding electrochromic, optochromic, and gaschromic properties.[1−3] With those distinctive properties, tungsten oxides have been used to make flat panel displays, photoelectrochromic smart windows and gas sensors.[1−3] Non-fully oxidized tungsten oxides (WO_{3-x}), such as $W_{20}O_{58}$, $W_{18}O_{49}$ and WO_2, are of particular interest because of their unique electronic characteristics, e.g. tungsten oxide has been found to be a semiconductor, a conductor or a superconductor in different oxidization states.[4,5] Since one-dimensional tungsten oxide nanomaterials exhibit superior properties in some promising applications[6−8] compared with bulk materials, much effort has been made to synthesize tungsten oxide nanowires by using different methods,[6−15] including a soft-chemistry approach,[9] the chemical vapour deposition (CVD) method,[7,8,12,14,15] hot-filament-assisted synthesis,[10] flame synthesis[11] and multistage field enhancement of tungsten oxide nanowires.[6] However, the electrical transport properties of tungsten oxide nanowires, which play an important role in their potential application to electronic nanodevices, are little reported. In the present paper, the electrical properties of a kind of tungsten oxide, $W_{18}O_{49}$, nanowires are investigated.

In the present paper, we report on a fabrication process of $W_{18}O_{49}$ nanowires on a tungsten rod substrate by using the CVD method with the aid of tin powders for the first time. The role of tin powders and the growth mechanism of the nanowires are studied. To investigate the electrical properties of the nanowires, *I–V* curves are measured by *in situ* TEM in which a tungsten tip that is movable in three dimensions, driven by piezoelectric ceramics, serves as an electrode and the tungsten rod substrate on which the nanowires are directly grown functions as another electrode, guaranteeing good contacts between the electrodes and the nanowire, so the electrical properties of the tungsten oxide nanowires can be obtained reliably. The experimental *I–V* curves are well fitted by using a metal–semiconductor–metal (MSM) model[16] and the intrinsic parameters of the tungsten oxide nanowires are retrieved.

*Project supported by the National Natural Science Foundation of China (Grant No 50671053).

†Corresponding author. E-mail: jzhu@mail.tsinghua.edu.cn

2. Experiment

To prepare tungsten oxide nanowires on a tungsten rod substrate, tungsten rods (Φ 0.3 mm) were immersed in 2.5 mol/L NaOH solution for 10 h to remove the surface oxide layer and then washed three times in de-ionized water. The tungsten oxide nanowires were grown by using the CVD method. A corundum tube furnace of 4 cm diameter was used. The tungsten rod substrate on an alumina boat was placed in the central part of the furnace immediately after being washed in de-ionized water. Tin powders ($\geq$ 99.5%) of 0.5 g were placed at the upstream end of the alumina boat. The furnace was heated to 850 °C, kept there for 2 h, then finally cooled down to room temperature. The total process was in an Ar atmosphere (99.999%) with a flow rate of 150 sccm (where sccm stands for standard-state cubic centimeter per minute).

As-synthesized nanowires were characterized by using a scanning electron microscope (SEM) (JEOL JSM-6301F), an energy-dispersive x-ray spectroscope (EDS) and a transmission electron microscope (TEM) (JEOL JEM-2010F). The *in situ* electrical properties of the nanowires were measured by using a Nanofactory TEM-scanning tunneling microscope (STM) specimen holder inside the TEM.

3. Results and discussion

Figure 1 shows an SEM image and an EDS spectrum of the nanowires on the tungsten rod substrate. Their diameters range from 7 to 200 nm and are uniform along their lengths, which range from 1 to 5 μm. The EDS spectrum shows that there is only tungsten and oxygen in the region where the nanowires are grown, which indicates that the synthesized one-dimensional nanomaterials are tungsten oxide nanowires. The nanowires were scraped from the tungsten rod substrate, dispersed in ethanol and then dripped onto a copper grid for TEM analysis.

TEM images shown in Fig.2 reveal that the tungsten oxide nanowires are single-crystalline. The selected area electron diffraction (SAED) pattern inset in Fig.2(b) was indexed as crystalline $W_{18}O_{49}$ according to JCPDS card No.71-2450. The spacings between the two perpendicular planes in the high resolution TEM (HRTEM) image shown in Fig.2(b) were measured to be 0.38 nm and 0.37 nm and the lattice planes could be best indexed as (010) and (103) of monoclinic $W_{18}O_{49}$, respectively, which confirms the index of the SAED pattern. The growth direction of the nanowires is the [010] direction of monoclinic $W_{18}O_{49}$ crystalline, which is reasonable because the close-packed planes of monoclinic $W_{18}O_{49}$ are {010}.

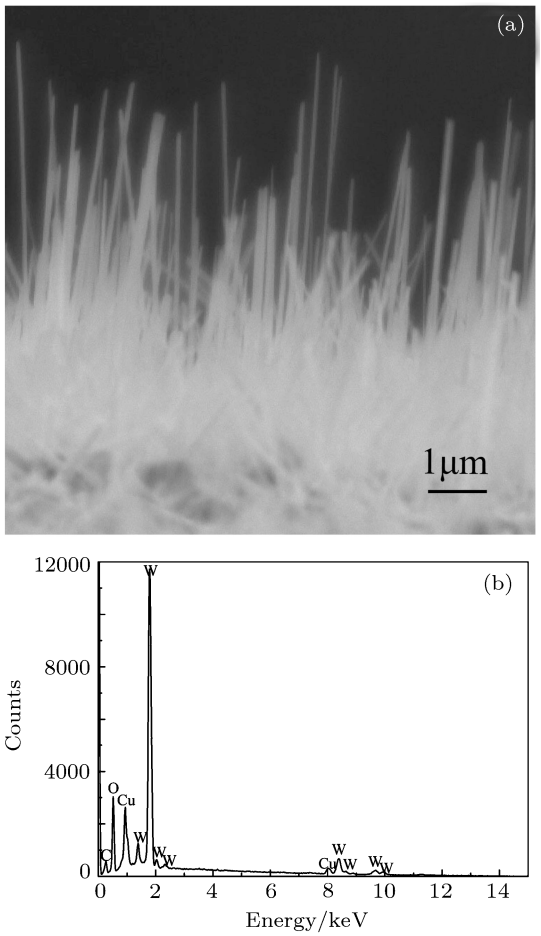


Fig.1. (a) SEM image and (b) EDS spectrum of the nanowires on the tungsten rod substrate. In the EDS spectrum, W and O signals come from the nanowires and Cu and C signals originate from the specimen holder and the contamination in the SEM column, respectively.

According to the TEM and the SEM observations, tin nanoparticles are not observed at the top of the $W_{18}O_{49}$ nanowires, which implies that the tin powders do not act as a catalyst. Therefore, the nanowire growth is unrelated to the vapour–liquid–solid (VLS) mechanism in which the nanowire grows from a liquified metal catalyst nanoparticle. To explore the growth mechanism of the nanowires and the role of the tin powders, a series of experiments with and without tin powders at different Ar flow rates were carried out (see Table 1). All of those experiments were carried out after the furnace had been heated to 850 °C and kept there for 2 h.

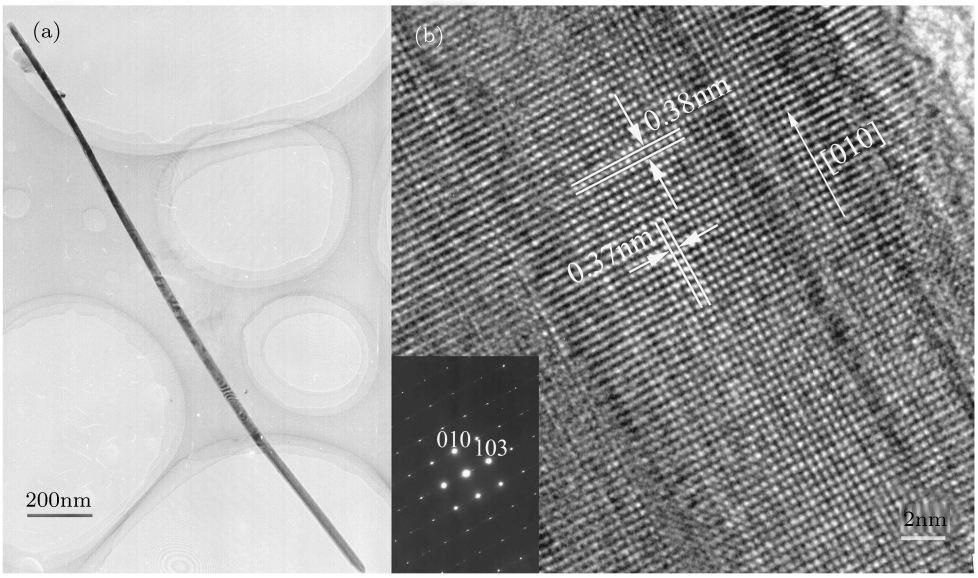


Fig.2. TEM images of a $W_{18}O_{49}$ nanowire: (a) Bright field image, (b) HRTEM image. The inset in Fig.2(b) shows the corresponding SAED pattern.

Table 1. Experimental results with and without tin powders, at different flow rates of Ar.

flow rate of Ar /sccm	with 0.5 g tin powders	without tin powders
50	No	No
100	No	No
150	Yes	No
200	No	No

Yes (No) means the $W_{18}O_{49}$ nanowires were (not) grown in experiment.

It can be seen from Table 1 that the $W_{18}O_{49}$ nanowires grew on the tungsten rod substrates in the experiment only with tin powders of 0.5 g and at an Ar flow rate of 150 sccm but not in the experiments without tin powders, no matter what the flow rate of Ar used was as shown in Fig.3. According to the previous studies,[6,7,12] $W_{18}O_{49}$ nanowires were prepared on tungsten substrates in an atmosphere containing an extremely low oxygen concentration (about 10^{-1} sccm) or in vacuum. It should be noted that the oxygen leakage of our system was found to be about 3 sccm. Due to the high oxygen level, the tungsten oxide nanowires are not expected to form without the aid of tin powders. When the tin powders were added into the furnace, they tended to react with oxygen to form tin oxide, which would significantly lower the oxygen concentration in the furnance. Experimentally, the tin oxides were found in the upstream zone of the area where the $W_{18}O_{49}$ nanowires grew. Based on the above analysis, it is highly possible that the role of the tin powders in our experiments is to control the oxygen concentration in the furnace by the reaction of the tin with oxygen and to assist the nanowire in its growth. With the increase of the Ar flow rate, more liquid tin reacted with oxygen. An appropriate oxygen concentration for the growth of tungsten oxide nanowires was reached at an Ar flow rate of 150 sccm, and the tungsten on the substrate surface reacting with the residual oxygen formed the $W_{18}O_{49}$ nanowires mainly through the VS mechanism.[17] When the Ar flow rate was increased to 200 sccm, the formed tin oxide covered most of the surface of the tungsten rod substrate, leading to the failure of the VS mechanism. As a result, few nanowires were found on the substrate. Zinc powders which also have low melting point were used, too. Zinc oxide nanowires, unlike tungsten oxide nanowires, grew on a tungsten rod substrate at an Ar flow rate of 150 sccm, which may result from the fact that zinc oxide has good crystallization compared with tungsten oxides and this affects the growth of tungsten oxide nanowires.

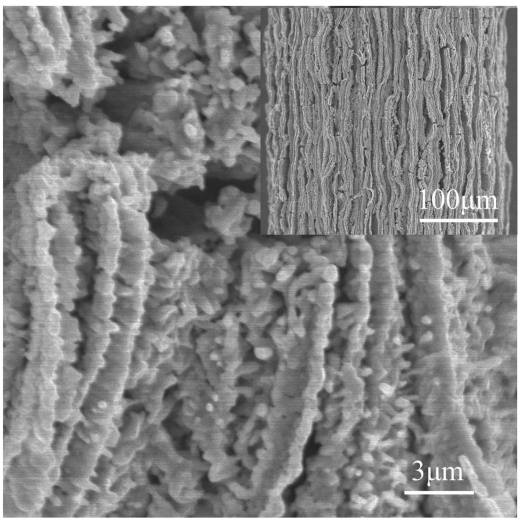


Fig.3. Typical SEM images of the tungsten rod substrate surface in the experiment without tin powders, and the inset is an SEM image with low magnification.

To investigate the electrical properties of the synthesized $W_{18}O_{49}$ nanowires, *in situ* I–V measurements were carried out inside the TEM. Figure 4 shows a TEM image of the electrical measurement geometry of a $W_{18}O_{49}$ nanowire. A movable tungsten tip electrode driven by piezoelectric ceramics is in contact with one end of the nanowire, and the tungsten rod substrate on which the nanowire is directly grown



Fig.4. TEM image of *in situ* two-terminal I–V measurement of a $W_{18}O_{49}$ nanowire.

serves as another electrode. The chemical connection of the tungsten rod substrate with the nanowire is much better than the physical contact, realized by van der Waals force, between the platinum rod electrode and the zinc oxide nanowire in the previous work.[16] Therefore, good contacts between the electrodes and the tungsten oxide nanowire are achieved. True I–V response can thus be acquired easily. Note that the resistance of the tungsten oxide layer on the surface of the tungsten rod substrate can be neglected because the tungsten oxide layers on the surface of the substrate and the tungsten rod in the central section of the substrate are connected in parallel in the circuit, and the resistance of the former is much larger than that of the latter.

Generally, the I–V characteristics of nanowires are linear,[18,19] rectifying,[20−23] asymmetric[24−26] or symmetric.[24,27,28] The characteristics of I–V curves are determined by the contacts between the two metal electrodes and the nanowire rather than by the nanowire itself.[16] The contact between a metal electrode and a nanowire can be either a Schottky barrier or an Ohmic contact. In turn, the characteristics of I–V curves can reveal the type of contacts between the metal electrodes and the nanowire. A linear I–V curve indicates that both of the contacts between the two metal electrodes and the nanowire are Ohmic contacts. A rectifying I–V curve shows that one contact is an Ohmic contact and the other is a Schottky barrier. A symmetric or an asymmetric I–V curve reveals that both of the contacts are Schottky barriers. Figure 5 shows the symmetric I–V

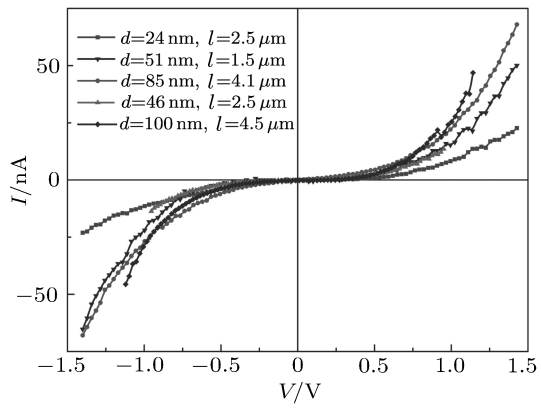


Fig.5. Symmetric I–V curves of five $W_{18}O_{49}$ nanowires, where d and l represent the diameter and the length of the nanowire, respectively.

curves of five tungsten nanowires with different diameters in our experiments, while linear, rectifying and asymmetric curves are not observed. The symmet-

ric I–V curves exhibit the existence of Schottky barriers between the metal electrodes and the $W_{18}O_{49}$ nanowires. Therefore, the $W_{18}O_{49}$ nanowires synthesized in our experiments are semiconducting. Two tungsten electrodes and a $W_{18}O_{49}$ nanowire in between constitute an MSM structure. The MSM structure will be depicted in detail below.

A schematic diagram of our MSM structure and its equivalent circuit for Fig.4 are shown in Fig.6. An Ohmic contact can be regarded as a Schottky barrier of zero barrier height. Therefore, the MSM structure is equivalent to two back-to-back Schottky barriers each connected with one end of a resistor in between (see Fig.6).

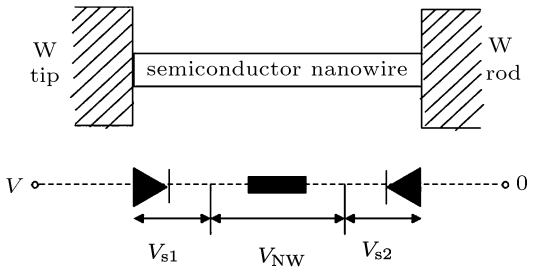


Fig.6. A schematic diagram of our MSM structure and its equivalent circuit (dash line)

When a negative voltage V is applied to the left electrode — the tungsten tip, the left Schottky barrier is reverse biased and the right Schottky barrier is forward biased. The voltages on the reverse-biased Schottky barrier, the forward-biased Schottky barrier and the $W_{18}O_{49}$ nanowire are denoted as V_{s1}, V_{s2} and V_{NW}, respectively as shown in Fig.6. Then

$$V = V_{s1} + V_{NW} + V_{s2}. \tag{1}$$

According to the thermionic-emission theory,[29] the reverse current of an ideal Schottky barrier should saturate at a very low value which is usually negligible. Therefore, a Schottky diode is regarded as being "off" at a reverse bias. However, for symmetric I–V curves, the reverse current is comparable with the forward current, indicating that the current tunneled through the reverse-biased barrier, which could be explained by thermionic-field emission theory,[29,30] while the current transport of the forward-biased Schottky barrier still obeys the thermionic-emission theory.

According to the thermionic-field emission theory, the reverse tunneling current density through the left Schottky barrier is expressed as[29]

$$J_{s1}(V_{s1}, \phi_{b1}) = -J_s(V_{s1}, \phi_{b1}) \times \exp\left[V_{s1}\left(\frac{q}{kT} - \frac{1}{E_0}\right)\right], \tag{2}$$

where J_s varies slowly with applied bias and is given as

$$J_s = \frac{A^*T(\pi q E_{00})^{1/2}}{k} \exp\left(-\frac{\phi_{b1}}{E_0}\right) \times \left[q(V_{s1} - \xi) + \frac{q\phi_{b1}}{\cosh^2(qE_{00}/kT)}\right]^{1/2}, \tag{3}$$

and

$$E_0 = E_{00} \coth\left(\frac{qE_{00}}{kT}\right), \tag{4}$$

with

$$E_{00} = \frac{\hbar}{2}\left[\frac{N_d}{m_n^* \varepsilon_s \varepsilon_0}\right]^{1/2}. \tag{5}$$

Here, ϕ_{b1} is the effective Schottky barrier height including the effects of image force, surface state and field penetration on it; ξ is the distance from the Fermi energy to the bottom of the conduction band; q is the magnitude of electronic charge; k is the Boltzmann constant; $A^* = 4\pi m_n^* q k^2/h^3$ is the Richardson constant of the semiconductor; T is the absolute temperature; h and $\hbar$ are the Planck constants; N_d is the donor density in the metal/semiconductor interface; m_n^* is the effective mass of electron of the semiconducting nanowire; ε_s is the relative dielectric coefficient of the semiconducting nanowire; ε_0 is the dielectric coefficient of free space.

According to the thermionic-emission theory, the forward current density across the right Schottky barrier is expressed as[29]

$$J_{s2}(V_{s2}, \phi_{b2}) = A^*T^2 \exp\left(\frac{qV_{s2}}{nkT}\right) \exp\left(-\frac{q\phi_{b2}}{kT}\right) \times \left\{1 - \exp\left(-\frac{qV_{s2}}{kT}\right)\right\}, \tag{6}$$

where ϕ_{b2} is the effective Schottky barrier height including the effects of image force, surface state and field penetration on it, and n is the ideality factor for describing the deviation of the diode from an ideal Schottky barrier with $n = 1$.

The currents through the reverse-biased Schottky barrier, the nanowire and the forward-biased Schottky barrier should be the same, i.e.

$$I = S_1 J_{s1}(V_{s1}, \phi_{b1}) = V_{NW}/R = S_2 J_{s2}(V_{s2}, \phi_{b2}), \tag{7}$$

where S_1 and S_2 are the contact areas of the reverse-biased Schottky barrier and the forward-biased Schottky barrier, respectively, and they are assumed to be equal to the cross sectional area of the nanowire.

Substituting expression (2) into expression (7) yields

$$I = S_1\left\{-J_{\rm s}(V_{\rm s1},\phi_{\rm b1})\times\exp\left[V_{\rm s1}\left(\frac{q}{kT}-\frac{1}{E_0}\right)\right]\right\}, \quad (8)$$

thus

$$\ln I = \ln S_1 - \ln J_{\rm s}(V_{\rm s1},\phi_{\rm b1}) + V_{\rm s1}\left(\frac{q}{kT}-\frac{1}{E_0}\right). \quad (9)$$

Because $J_{\rm s}$ is insensitive to applied bias $V_{\rm s1}$, $\ln I - V_{\rm s1}$ is linear and the slope is $\left(\frac{q}{kT}-\frac{1}{E_0}\right)$.

The experimental I–V curve of a $W_{18}O_{49}$ nanowire with 19.2 nm diameter and 2.5 μm length was fitted by using the MSM model as indicated in Fig.7. In the MSM mode, the majority of the voltage drop is attributed to the reverse-biased Schottky barriers at medium bias, whereas the majority of the voltage drop is ascribed to the nanowire itself at high bias as shown in Fig.7(a). Therefore, the initial value of the significant tunneling parameter E_0 was calculated by using the slope of the $\ln I - V$ curve, $\left(\frac{q}{kT}-\frac{1}{E_0}\right)$, at medium bias ($2\,V < |V| < 3\,V$) to be 26.41 meV, i.e. $E_0 = 26.41$ meV and the resistance of the nanowire, R, was primarily determined from $R = \frac{{\rm d}V}{{\rm d}I}$ to be 9.32 MΩ, i.e. $R = 9.32$ MΩ, at large bias, $|V| > 8$ V, where the current varies linearly with voltage. E_0, R, $\phi_{\rm b1}$ and $\phi_{\rm b2}$ were further retrieved precisely by the MSM model through using the non-linear least-squares method and the simulated annealing approach.[27] We have obtained the following results: $E_0 = 26.11$ meV, $R = 7.63$ MΩ, $\phi_{\rm b1} = \phi_{\rm b2} = 0.31$ eV. It can be seen from Fig.7(b) that the fitted I–V curve is satisfactorily consistent with the experimental I–V curve. The conductivity of the nanowire, σ, was calculated according to its geometrical parameters of 19.2 nm diameter and 2.5 μm length, to be $\sigma = \frac{1}{\rho} = \frac{l}{RS} = 11.32$ S/cm. Using m^*[31] and $\varepsilon_{\rm s}$[32] of bulk $W_{18}O_{49}$ as the corresponding constants of the nanowire, the carrier concentration $N_{\rm d}$ was calculated according to expressions (4) and (5) to be $N_{\rm d} = 1.77\times10^{18}$ cm^{-3}. The carrier mobility μ was calculated from $\mu = \frac{\sigma}{N_{\rm d}q}$ and obtained as $\mu = 39.92$ cm$^2\cdot$V$^{-1}\cdot$s^{-1}.

The intrinic parameters of other $W_{18}O_{49}$ nanowires were also extracted precisely from their experimental I–V curves by using the MSM model. The average carrier mobility, the carrier concentration and the conductivity of the $W_{18}O_{49}$ nanowires were determined to be 70±30 cm$^2\cdot$V$^{-1}\cdot$S^{-1}, $3\times10^{17} - 2\times10^{18}$ cm^{-3} and 4–11 S/cm, respectively. Note that the variations in carrier concentration and conductivity are primarily due to the fluctuation of the ratio between surface area and volume of nanowires.

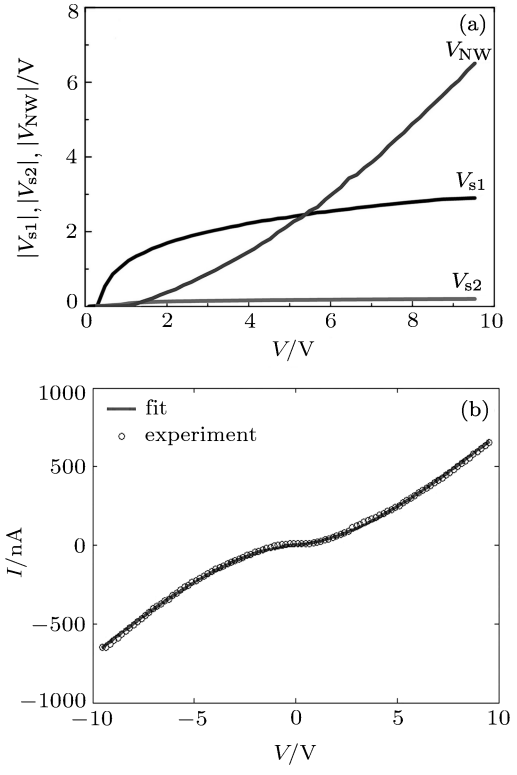


Fig.7. (a) Variations of $|V_{\rm s1}|$, $|V_{\rm NW}|$ and $|V_{\rm s2}|$ with applied voltage $|V|$, where resistance of the nanowire is 10 MΩ and contact barrier heights are both 0.31 eV, and (b) measured and fitted I–V curves.

4. Conclusions

The $W_{18}O_{49}$ nanowires are synthesized on the tungsten rod substrate by the CVD reaction in which tin powders are used to control oxygen concentration in the furnace and to aid the nanowires to grow. An appropriate flow rate of Ar and an extremely low oxygen concentration are essential for the $W_{18}O_{49}$ nanowire formation, which is still in the framework of the VS mechanism. The I–V curves of the $W_{18}O_{49}$ nanowires measured by using an *in situ* TEM are symmetric. The experimental I–V curves are well reproduced by using the MSM model and the intrinsic parameters of the nanowires are retrieved at the same time. Our data show that the $W_{18}O_{49}$ nanowires may have potential applications in electronic nanodevices.

References

[1] Liao C C, Chen F R and Kai J J 2006 *Sol. Energy Mater. Sol. Cells* **90** 1147

[2] Turyan I, Krasovec U O, Orel B, Saraidorov T, Reisfeld R and Mandler D 2000 *Adv. Mater.* **12** 330

[3] Solis J L, Saukko S, Kish L, Granqvist C G and Lantto V 2001 *Thin Solid Films* **391** 255

[4] Salje E K H and Eur J 1994 *Solid State Inorg. Chem.* **31** 651

[5] Aird A, Domeneghetti M C, Mazzi F, Tazzoli V and Salje E K H 1998 *J. Phys.: Condens. Matter* **10** L569

[6] Seelaboyina R, Huang J, Park J, Kang D H and Choi1 W B 2006 *Nanotechnology* **17** 4840

[7] Li Y B Bando Y and Golberg D 2003 *Adv. Mater.* **15** 1294

[8] Baek Y and Yong K 2007 *J. Phys. Chem.* C **111** 1213

[9] Polleux J Gurlo A Barsan N Weimar U Antonietti M and Niederberger M 2006 *Angew. Chem. Int. Ed.* **45** 261

[10] Thangala J Vaddiraju S Bogale R Thurman R Powers T Deb B and K Sunkara M 2007 *Small* **3** 890

[11] Xu F S, Tse S D, Al-Sharab J F and Kear B H 2006 *Appl. Phys. Lett.* **88** 243115

[12] Gu G Zheng B Han W Q Roth S and Liu J 2002 *Nano. Lett.* **2** 849

[13] Wang S L, He Y H, Zou J, Cao P, Jiang Y, Huang B Y, Liu C T and Liaw P K 2007 *J. Crystal Growth* **303** 574

[14] Hong K Q, Xie M H and Wu H S 2006 *Nanotechnology* **17** 4830

[15] Hong K Q, Xie M H, Hu R and Wu H S 2008 *Nanotechnology* **19** 085604

[16] Zhang Z Y, Jin C H, Liang X L, Chen Q and Peng L M 2006 *Appl. Phys. Lett.* **88** 73102

[17] Zhang Y J, Wang N L, Gao S P, He R R, Miao S, Liu J, Zhu J and Zhang X 2002 *Chem. Mater.* **14** 3564

[18] Lee Y H, Yoo J M, Park D H, Kim D H and Ju B K 2005 *Appl. Phys. Lett.* **86** 033110

[19] Cui Y, Duan X F, Hu J T and Lieber C M 2000 *J. Phys. Chem.* B **104** 5213

[20] Lao C S, Liu J, Gao P X, Zhang L Y, Davidovic D, Tummala R and Wang Z L 2006 *Nano. Lett.* **6** 263

[21] Heo Y W, Tien L C, Norton D P, Pearton S J, Kang B S, Ren F and LaRoche J R 2004 *Appl. Phys. Lett.* **85** 3107

[22] Fan Z Y and Lu J G 2005 *Appl. Phys. Lett.* **86** 032111

[23] Tang W H, Fu X L, Zhang Z Y and Li L H 2006 *Chin. Phys.* **15** 0773

[24] Wang D Q, Zhou Z Y, Zhu R and Ye X Y 2008 *Chin. Phys.* B **17** 3875

[25] Luo J, Xing Y J, Zhu J, Yu D P, Zhao Y G, Zhang L, Fang H, Huang Z P and Xu J 2006 *Adv. Funct. Mater.* **16** 1081

[26] Luo J, Zhu J, Huang Z P and Zhang L 2007 *Appl. Phys. Lett.* **90** 033114

[27] Liu Y Zhang Z Y, Hu Y F Jin C H and Peng L M 2008 *J. Nanosci. Nanotechnol.* **8** 252

[28] Long Y Z, Wang W L, Bai F L, Chen Z J, Jin Ai Z and Gu C Z 2008 *Chin. Phys.* B **17** 1389

[29] Rhoderick E H and Williams R H 1988 Metal–Semiconductor Contact (Oxford: Oxford University Press) p96, p128

[30] Padovani F A and Stratton R 1966 *Solid-State Electronics* **9** 695

[31] Polaczekt A, Pqkatai M and Obuszkot Z 1994 *J. Phys.: Condens. Matter* **6** 7909

[32] Deb S K 1973 *Philos. Mag.* **27** 801